Scripta Materialia 130 (2017) 174–177

Contents lists available at ScienceDirect

Scripta Materialia

journal homepage: www.elsevier.com/locate/scriptamat

Regular article

# Monolayer-thick TiO precipitation in V-4Cr-4Ti alloy induced by proton irradiation

A. Impagnatiello [a,b,*], S.M. Shubeita [b], P.T. Wady [b], I. Ipatova [a,b], H. Dawson [a], C. Barcellini [a,b], E. Jimenez-Melero [a,b]

[a] School of Materials, The University of Manchester, Manchester M13 9PL, UK
[b] Dalton Cumbrian Facility, The University of Manchester, Moor Row CA24 3HA, UK

ARTICLE INFO

*Article history:*
Received 25 September 2016
Received in revised form 24 November 2016
Accepted 2 December 2016
Available online xxxx

*Keywords:*
Refractory metal
Precipitation
Lattice defects
High-resolution electron microscopy
Nuclear fusion reactor

ABSTRACT

We have characterised to atomic resolution the mono-layer thick TiO-type precipitate induced by proton irradiation in V-4Cr-4Ti alloy at a dose of 0.3 dpa and a temperature of 350 °C. Its formation coincides with the coarsening radiation-induced interstitial $a/2\langle 111\rangle$ dislocation loops that are already present at 300 °C. The dislocation network induced by prior cold work is mostly recovered at 300 °C and 0.3 dpa, and is therefore expected to exert a minimal effect on the precipitate formation. This monolayer-thick precipitate constitutes an early stage in the radiation-induced aging process of V-4Cr-4Ti at low temperatures, and can potentially absorb additional light elements in reactor environments.



Vanadium-based alloys currently constitute advanced candidate materials for the first wall of future fusion reactors such as DEMO [1,2]. In particular, V-4Cr-4Ti alloy offers an outstanding combination of high-temperature strength and radiation resistance [3–5], coupled with low neutron activation [6,7] and corrosion resistance to liquid metal coolants [8–10]. However, the presence of relatively small amounts of light atoms in the matrix can drastically increase the ductile-to-brittle transition temperature, and consequently also the minimum temperature for safe use of this alloy in structural components of the reactor [11,12]. Ti acts as an effective scavenger for light elements by forming Ti(O,C,N) precipitates during the material's processing [13]. Cold working prior to annealing can be used to minimise the coarsening of the precipitates and increase the thermal creep resistance of the alloy [14]. Additionally, the interface of those nano-scale precipitates with the matrix can act as an effective sink for mobile lattice defects [15,16]. Therefore, the radiation–induced hardening and embrittlement that take place in V-4Cr-4Ti below 400 °C and at dose levels as low as 0.1–0.5 dpa can be reduced.

Neutron irradiation of V-4Cr-4Ti alloy at temperatures below 275 °C induces the formation of a high density of faulted dislocation loops with a Burgers vector of $a/2\langle 110\rangle$ and an average size of ~3 nm. These small dislocation loops present a barrier strength lower than the Orowan value for impenetrable obstacles during dislocation gliding, and facilitate the formation of 50 nm-wide cleared dislocation channels on {110} slip planes at those low temperatures. This channel formation causes a pronounced loss of strain capability and uniform elongation in the V-4Cr-4Ti alloy. At higher neutron irradiation temperatures, $a/2\langle 111\rangle$ unfaulted dislocation loops predominate in the microstructure. They attain a larger average size of ~200 nm, whereas their density is reduced to $<10^{20}$ $m^{-3}$ [17]. In parallel to the occurrence and evolution of dislocation loops with temperature, recent positron annihilation results revealed the presence of Ti-vacancy complexes in the vicinity of the radiation-induced dislocation loops below 300 °C [18]. These complexes may act as precursors for the formation at higher temperatures of Ti-rich radiation-induced precipitates (RIPs). The growth of the additional precipitates induced by radiation may occur by changing their morphology from sphere to platelet, and also the O/Ti ratio [19]. And enhanced V content has also been reported in some of these RIPs [20]. Despite the key role of the RIPs in improving the radiation resistance of V-4Cr-4Ti in the low temperature regime, a detailed characterisation of their structure and elemental content, especially at the interface with the surrounding matrix, would allow the development of alloy microstructures with improved radiation resistance. The potential effect of pre-existing dislocations due to prior cold working on the precipitate formation should also be assessed. In this paper, we address these points by using proton irradiation as a surrogate to neutron damage, in combination with high-resolution electron microscopy to characterise both the RIPs and the presence of dislocation

* Corresponding author at: Dalton Cumbrian Facility, University of Manchester, Westlakes Science & Technology Park, Moor Row CA24 3HA, UK.
*E-mail address:* andrea.impagnatiello@postgrad.manchester.ac.uk (A. Impagnatiello).

http://dx.doi.org/10.1016/j.scriptamat.2016.12.002
1359-6462/

structures in the matrix. This study provides a comparison of proton irradiated microstructures with and without prior cold work. Generally speaking for other types of materials, the presence of dislocations due to cold work would favourably increase radiation resistance at relatively low dpa levels, since the dislocations would trap and slow down the diffusion of radiation-induced point defects [21,22]. Cold work can also be caused by the manufacturing of the reactor components, so understanding the effect of cold work on materials that will be under irradiation becomes even more important.

Equivalent V-4Cr-4Ti (wt.%) samples were solution-annealed (SA) at 1100 °C for 2 h and afterwards water quenched to room temperature. Some of the material was subsequently 10% cold rolled (SACW). The sample surface was ground to 4000 grit SiC paper, and then electro-polished using an electrolyte of 60 vol.% methanol–35 vol.% 2-buthoxyethanol–5 vol.% perchloric acid (60%) at a temperature of −35 °C. After that, the samples were irradiated with a 1.4 MeV proton beam produced using the 5MV tandem ion accelerator of the Dalton Cumbrian Facility [23]. The beam current deposited on the samples was ~28 μA, and the damage rate was $3 \times 10^{-6}$ dpa/s. We achieved a particle flux of $\sim 8.7 \times 10^{17}$ protons/m$^2$ s. The value of proton fluence of $\sim 8 \times 10^{22}$ particles/cm$^2$ is close to the fluence of $\sim 10^{24}$ neutrons/cm$^2$ from previous neutron irradiations of V-4Cr-4Ti samples [17]. The temperature during irradiation (either 300 or 350 °C) was monitored both with welded thermocouples on the sample surface adjacent to the irradiated area, and also with a non-contact pyrometer. For transmission electron microscope (TEM) imaging and analysis, discs were prepared by mechanical pre-thinning, followed by electro-polishing using the same electrolyte and temperature as previously mentioned. In order to characterise the damaged structure, we used a FEI Tecnai T20 with $LaB_6$ crystal and an FEI Titan G2 80-200 aberration-corrected S/TEM with an X-FEG and ChemiSTEM™ technology [24], both microscopes operating at 200 kV. The thickness of the disc area studied by TEM was derived from the fringes spacing of the convergent beam electron diffraction pattern, the interstitial or vacancy nature of the defects using the inside-outside method, and the Burgers vector from the $\mathbf{g}.\mathbf{b} = 0$ invisibility criterion [25,26]. Vickers hardness measurements were taken using a load of 0.025 g, resulting in an indentation depth of ~8 μm, which is close to the 60% of the Bragg peak position from the irradiated sample surface.

The initial (SA) microstructure contained a fine dispersion of plate-like Ti(O,C,N) precipitates [27], together with a number of cuboidal Ti-rich precipitates decorating the grain boundaries of the matrix. Fig. 1a shows a scanning electron micrograph of the cross section of the SA sample surface irradiated at 350 °C. The large plate-like precipitates formed during prior annealing treatment are clearly visible in the image. A relatively bright line at ~15 μm below the sample surface can be observed passing through two neighbouring grains of the matrix. The position of this bright line agrees well with the Bragg peak position of 14 μm calculated using the SRIM software [28], see Fig. 1b. In the region of the Bragg peak, the lattice is mostly damaged, the channelling of electrons is more impeded and therefore the BSE signal increases. We have prepared TEM discs of the irradiated samples at a depth of 60% of the Bragg peak position from the sample surface. This corresponded approximately to an 8 μm depth from the surface and a damage dose of 0.3 dpa in the studied samples.

Fig. 2 shows the TEM images of the SA and SACW samples, both before and after having been irradiated up to 0.3 dpa at a constant temperature of 300 °C. Before irradiation and cold work, the prior annealing at 1100 °C led to a microstructure free from the dislocation networks and other defects that are instead present after 10% cold work. After irradiation, dislocation loops are present in the SA sample with a density of $\sim 11 \times 10^{21}$ m$^{-3}$. The majority of these loops have a Burgers vector of $a/2\langle 111\rangle$ and their average size is 12 nm. A slightly lower density of dislocation loops is present in the SACW sample after irradiation, namely $\sim 9 \times 10^{21}$ m$^{-3}$, and their average diameter of 14 nm is close to the value for the SA sample. It is remarkable that the pre-existing dislocation network in the SACW sample is mostly recovered after irradiation.

The damaged microstructure of the SA sample after irradiation up to 0.3 dpa at 350 °C is shown in Fig. 3a. Interstitial $a/2\langle 111\rangle$ dislocation loops are also present in the microstructure. They are characterised by a larger average diameter of 86 nm and a lower density of $\sim 2 \times 10^{21}$ m$^{-3}$, as compared to the dislocation loops observed at 300 °C. However, at 350 °C we also observed new plate-shaped RIPs, oriented along the {100} planes of the V matrix. They appear with an average length of 56 nm and a density of $\sim 1.5 \times 10^{21}$ m$^{-3}$. Fig. 3b and c shows a higher-resolution image of the RIPs. The precipitates seem to be composed of only one atomic layer. Chemical analysis using energy-dispersive spectroscopy confirmed the presence of Ti [27]. These results suggest that these observed RIPs correspond to TiO-type precipitates with a lattice parameter of 0.42 nm [29] and the Baker–Nutting orientation relationship with the matrix [30]: $[001]_{TiO}//[001]_V$, $(110)_{TiO}//(100)_V$. This assumption allows us to propose in Fig. 3e–f a crystal model of the plate-like precipitates that is consistent with the atomic resolution TEM data of Fig. 3c–e.

Table 1 summarises the microstructure of the irradiated samples in terms of average length and density of RIPs and dislocation loops, together with the change in hardness due to irradiation. The number of dislocation loops in the SACW sample is somewhat lower than in the SA at 300 °C. The presence of the dislocation network in the SACW sample may have reduced the mobility of the radiation-induced point defects that eventually form dislocation loops. As reported for cold-worked irradiated steels, a significant reduction of the initial dislocation network is required for the development of observable dislocation loops [31]. Irradiation at intermediate doses would be required to understand the evolution of pre-existent dislocations to achieve their full recovery at the relatively low temperature of 300 °C. In this alloy recovery occurs during annealing above 400 °C in the absence of irradiation [32]. Furthermore, the hardness values of the SA and SACW samples after irradiation at 300 °C lie very close. This is due to their dislocation structures

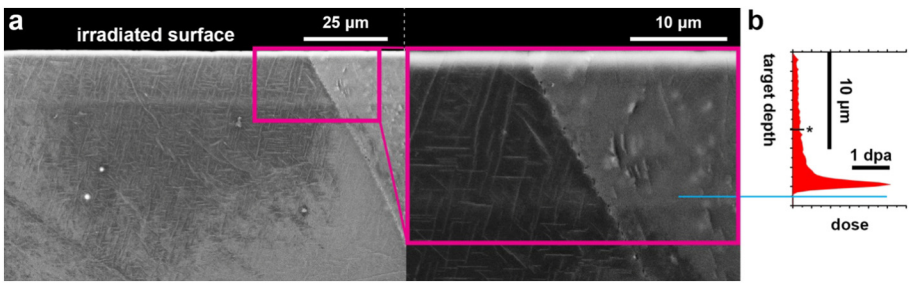


**Fig. 1.** (a) SEM (BSE, 30 keV) image of the cross section of the solution-annealed V-4Cr-4Ti alloy irradiated up to 0.3 dpa at 350 °C, and (b) simulated damage profile using the SRIM software with the quick Kinchin–Pease approach [40] and the total current deposited on the sample during the irradiation experiment. The asterisk locates the depth equal to 60% the Bragg peak position, and denotes the region in the sample from where TEM foils were prepared.

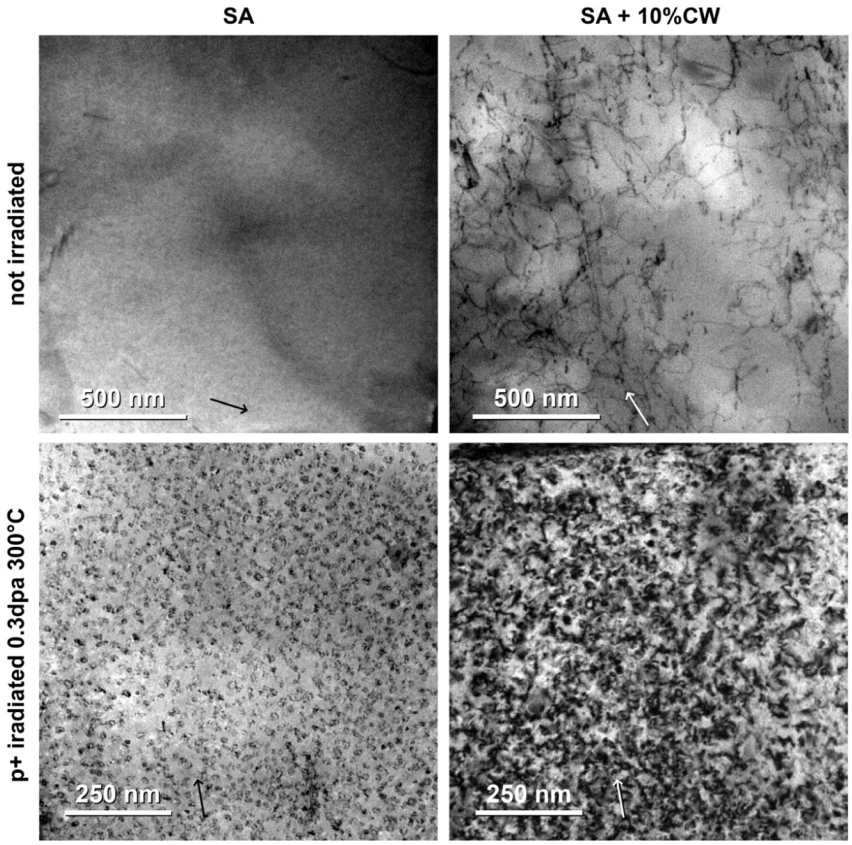


**Fig. 2.** TEM images of the microstructure of the solution annealed (SA) and SA + 10% cold worked (CW) samples, before and after proton irradiation up to 0.3 dpa at 300 °C. The arrows show the **g** 200 direction.

after irradiation being also very similar. Taking into account that the cold work raised the hardness of the material before irradiation, the hardness change after irradiation seems to decrease with the amount of cold work prior irradiation. In conclusion it appears that the initial 10% cold work does not affect significantly the final hardness of the alloy after irradiation.

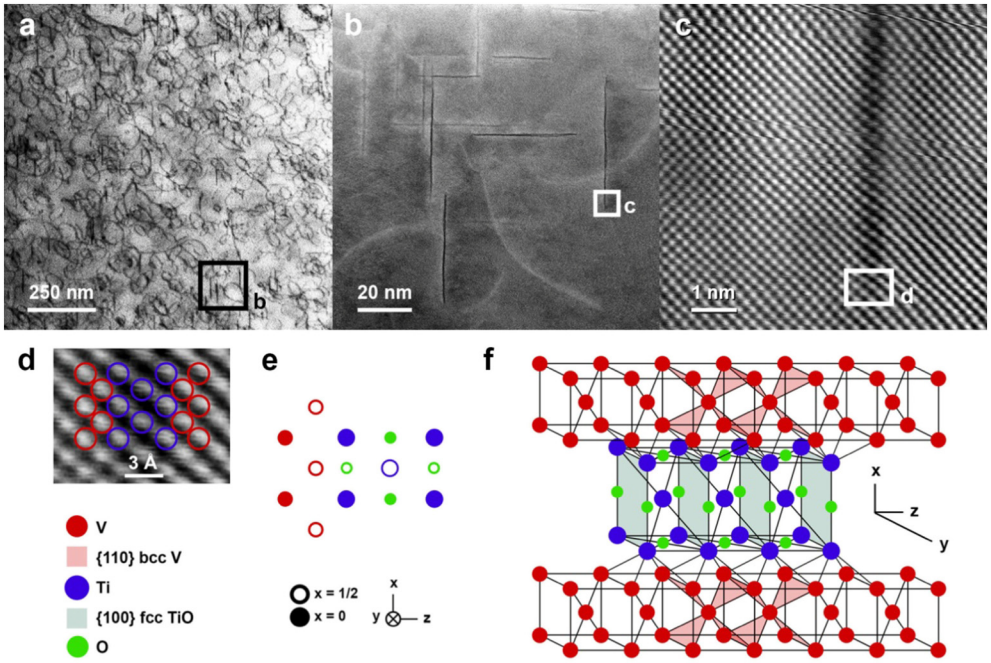


**Fig. 3.** (a) Microstructure of the solution-annealed sample after undergoing proton irradiation up to 0.3 dpa at 350 °C, (b) detail from (a) of Ti-rich radiation induced precipitates aligned along the [100] direction of the vanadium matrix, together with a number of dislocation loops, (c) atomic-resolution image of the region outlined by the square in (b), (d) atomic-resolution detail of the region outlined by the square in (c) where the position of the Ti and V atoms are indicated by blue and red circles, respectively, (e) upper and (f) 3-D view of the crystal structure model of the plate-like precipitate shown in (c) and (d). (a) was obtained in TEM mode, whereas the (b–d) were collected in STEM mode. In all images, B = [001] and **g** 200 lies parallel to the scale bar. (For interpretation of the references to colour in this figure legend, the reader is referred to the web version of this article.)

**Table 1**
Average length/size and density of the dislocation loops and irradiation-induced Ti-rich precipitates observed in the irradiated V-4Cr-4Ti samples together with the initial hardness value ($HV_i$) and the change in hardness due to proton irradiation ($\Delta HV_{irr}$).

| Sample condition | $HV_i$ | $T_{irr}$ (°C) | Dose (dpa) | $\Delta HV_{irr}$ | Dislocation loops | | Irr. induced precipitates | |
|---|---|---|---|---|---|---|---|---|
| | | | | | Average size (nm) | Density $\times 10^{21}$ m$^{-3}$ | Average length (nm) | Density $\times 10^{21}$ m$^{-3}$ |
| SA | 196 ± 8 | 300 | 0.3 | 130 ± 19 | 12 | 11 | – | – |
| | 196 ± 8 | 350 | 0.3 | 90 ± 18 | 85 | 2 | 56 | 1.5 |
| SA + 10% CW | 217 ± 13 | 300 | 0.3 | 104 ± 26 | 14 | 9 | – | – |

Dislocation loops found in all the irradiated samples were of interstitial nature, consistent with previous work on neutron irradiated V-4Cr-4Ti in this temperature range [17]. They are unfaulted and the predominant Burgers vector is $a/2\langle 111\rangle$. Faulted dislocation loops with a Burgers vector of $a/2\langle 110\rangle$ were reported for temperatures below 300 °C in previous neutron-irradiation studies [17]. Molecular dynamic simulations previously showed that this latter type of dislocation loop has a relatively high formation energy and become unstable at high temperatures [33]. We found that the increase in irradiation temperature from 300 °C to 350 °C causes a reduction in the density of dislocation loops and an increase in the average size of the loops. As a consequence, the irradiation-induced hardening of the alloy ($\Delta HV_{irr}$) diminishes with increasing temperature above 300 °C, see Table 1. A higher density of finer loops at 300 °C implies more obstacles to the motion of dislocations and, as a consequence, an enhanced irradiation hardening [34]. The decrease in hardening due to the temperature evolution of the dislocation structure is partially compensated by the appearance of RIPs at 350 °C [35]. Differences in dose rate between neutron and proton irradiation are expected to yield a lower average loop size in the proton irradiated specimens (~85 nm) as compared to neutron irradiation (~200 nm) [36].

The appearance of Ti-rich RIPs at a radiation dose of 0.3 dpa occurred between 300 °C and 350 °C, in agreement with previous neutron irradiation experiments [18]. In non-irradiated conditions, the formation plate-like Ti(O,C,N) precipitates is induced above 500 °C by climbing dislocations during recovery [37]. Proton irradiation at lower temperatures has triggered the formation of dislocation loops, and at 350 °C also the formation of additional plate-like TiO-type precipitates. The radiation-induced mobile vacancies would increase the diffusion of substitutional Ti atoms, and the occurrence of Ti-vacancy complexes close to the dislocation loops, where the additional TiO-type precipitates form [17,18]. The crystal structure model in Fig. 3e describes the precipitate platelet as an fcc TiO monolayer, whose interface with the V matrix is coherent along the sides of the platelet. This monolayer platelet could evidence that the proposed Ti spherical clusters [19] evolve to a platelet Guinier-Preston (GP) zone visible with TEM techniques. The GP zone would finally evolve to a thicker plate as the dose is increased. The thickness of these TiO-type plates has been reported to be ~1–3 nm at a neutron radiation dose of 4 dpa and a temperature of ~510 °C [38]. This precipitation sequence is similar to the precipitation behaviour observed in Al-Cu alloys during annealing at 130 °C, where monolayer, bilayer and multilayer Cu-rich plate-like precipitates correspond to different stages of hardening during aging [39]. Therefore, the initial Ti-vacancy clusters, the monolayer platelet reported in this work, and the multilayer TiO-type precipitates characterise different stages of radiation-induced precipitation hardening in the V-4Cr-4Ti alloy.

In conclusion, our results on proton-irradiated V-4Cr-4Ti alloy lie in accordance with the nature and evolution of dislocation loops observed in the same alloy irradiated with neutrons at equivalent temperatures. Our TEM data also revealed that the dislocation networks induced by prior cold work are mainly recovered at 300 °C and a radiation dose of 0.3 dpa. Therefore those pre-existing dislocations exert a minor effect on the formation of radiation-induced TiO-type plate precipitates observed at 350 °C. Our high-resolution TEM data allowed us to characterise the monolayer-thick TiO precipitate. This precipitate constitutes an early stage in the radiation-induced aging process of V-4Cr-4Ti at relatively low temperatures, and therefore possesses the capacity of absorbing additional light elements in fusion reactor operation conditions.

We acknowledge the Engineering and Physical Sciences Research Council (EPRSC) (EP/K504178/1) for providing funding for this project via the Centre for Doctoral Training in the Science and Technology of Fusion Energy (http://www.fusion-cdt.ac.uk/). The work described was supported in part by the Dalton Cumbrian Facility Project, a joint initiative of The University of Manchester and the Nuclear Decommissioning Authority. We would also like to thank A.D. Smith and N. Mason for their assistance during the irradiation experiment.

## References

[1] J.M. Chen, V.M. Chernov, R.J. Kurtz, T. Muroga, J. Nucl. Mater. 417 (2011) 289.
[2] T. Muroga, J.M. Chen, V.M. Chernov, R.J. Kurtz, M. Le Flem, J. Nucl. Mater. 455 (2014) 263.
[3] K. Fukumoto, T. Morimura, T. Tanaka, A. Kimura, K. Abe, H. Takahashi, et al., J. Nucl. Mater. 239 (1996) 170.
[4] T. Muroga, J.M. Chen, V.M. Chernov, K. Fukumoto, D.T. Hoelzer, R.J. Kurtz, et al., J. Nucl. Mater. 367-370 (2007) 780.
[5] F.A. Garner, T. Okita, N. Sekimura, J. Nucl. Mater. 417 (2011) 314.
[6] D.L. Smith, M.C. Billone, K. Natesan, Int. J. Refract. Met. Hard Mater. 18 (2000) 213.
[7] D.V. Markovskij, Fusion Eng. Des. 51-52 (2000) 695.
[8] R.L. Ammon, Int. Met. Rev. 5 (1980) 255.
[9] B.A. Pint, J.L. Moser, P.F. Tortorelli, Fusion Eng. Des. 81 (2006) 901.
[10] I.V. Borovitskaya, I.E. Lyublinski, V.V. Paramonova, S.N. Korshunov, A.N. Mansurova, M.M. Lyakhovitskiy, et al., Inorg. Mater. Appl. Res. 6 (2015) 133.
[11] S.J. Zinkle, N.M. Ghoniem, Fusion Eng. Des. 51-52 (2000) 55.
[12] A.-A. Tavassoli, J. Nucl. Mater. 302 (2002) 73.
[13] D.R. Diercks, B.A. Loomis, J. Nucl. Mater. 141-143 (1986) 1117.
[14] T. Muroga, T. Nagasaka, P.F. Zheng, J.M. Chen, Adv. Sci. Technol. 73 (2010) 22.
[15] M.S. Staltsov, I.I. Chernov, B.A. Kalin, K.Z. Oo, A.A. Polyansky, O.S. Staltsova, et al., J. Nucl. Mater. 461 (2015) 56.
[16] A. van Veen, A.V. Fedorov, A.I. Ryazanov, J. Nucl. Mater. 258-263 (1998) 1400.
[17] P.M. Rice, S.J. Zinkle, J. Nucl. Mater. 258-263 (1998) 1414.
[18] K.-i. Fukumoto, H. Matsui, H. Ohkubo, Z. Tang, Y. Nagai, M. Hasegawa, J. Nucl. Mater. 373 (2008) 289.
[19] N. Nita, Y. Anma, H. Matsui, T. Ohkubo, K. Hono, J. Nucl. Mater. 367 (2007) 858.
[20] M. Hatakeyama, T. Nagasaka, T. Muroga, T. Toyama, I. Yamagata, J. Nucl. Mater. 442 (2013) S346.
[21] S.J. Zinkle, L.L. Snead, Annu. Rev. Mater. Res. 44 (2014) 241.
[22] J.O. Stiegler, E.E. Bloom, J. Nucl. Mater. 41 (1971) 341.
[23] P.T. Wady, A. Draude, S.M. Shubeita, A.D. Smith, N. Mason, S.M. Pimblott, et al., Nucl. Instr. Meth. Phys. Res. A 806 (2016) 109.
[24] D. Sudfeld, O. Lourie, S. Kujawa, J. Phys. Conf. Ser. 522 (2014) 012026.
[25] S.M. Allen, Philos. Mag. A 43 (1981) 325.
[26] M.L. Jenkins, M.A. Kirk, Characterization of Radiation Damage by Transmission Electron Microscopy, Institute of Physics Publishing, 2001.
[27] A. Impagnatiello, D. Hernandez-Maldonado, G. Bertali, E. Prestat, D. Kepaptsoglou, Q. Ramasse, et al., Scr. Mater. 126 (2017) 50.
[28] J.F. Ziegler, M.D. Ziegler, J.P. Biersack, Nucl. Instrum. Meth. B 268 (2010) 1818.
[29] K.H. Kramer, J. Less-Common Met. 21 (1970) 365.
[30] J.W. Edington, Practical Electron Microscopy in Materials Science, Gloeilampenfabrieken, Eindhoven, 1975.
[31] S.J. Zinkle, P.J. Maziasz, R.E. Stoller, J. Nucl. Mater. 206 (1993) 266.
[32] A.N. Gubbi, A.F. Rowcliffe, J. Nucl. Mater. 233 (1996) 497.
[33] L.A. Zepeda-Ruiz, J. Marian, B.D. Wirth, Philos. Mag. 85 (2005) 697.
[34] K.-i. Fukumoto, H. Matsui, H. Tsai, D.L. Smith, J. Nucl. Mater. 283 (2000) 492.
[35] K.-i. Fukumoto, H. Matsui, Y. Candra, K. Takahashi, H. Sasanuma, S. Nagata, et al., J. Nucl. Mater. 283 (2000) 535.
[36] C. Abromeit, J. Nucl. Mater. 216 (1994) 78.
[37] T. Leguey, R. Pareja, J. Nucl. Mater. 279 (2000) 216.
[38] D.T. Hoelzer, S.J. Zinkle, DOE/ER-0313/29, 2000 19.
[39] S.K. Son, M. Takeda, M. Mitome, Y. Bando, T. Endo, Mater. Lett. 59 (2005) 629.
[40] ASTM E521-96, Standard Practice for Neutron Radiation Damage Simulation by Charged-particle Irradiation, 2009.